JOURNAL OF SPACECRAFT AND ROCKETS
Vol. 43, No. 1, January–February 2006

Chemical and Solar-Electric-Propulsion Systems Analyses for Mars Sample Return Missions

Benjamin B. Donahue*
Boeing Phantom Works, Huntsville, Alabama 35806
Shaun E. Green†
Science Applications International Corporation, Huntsville, Alabama 35806
and
Victoria L. Coverstone‡ and Byoungsam Woo§
University of Illinois at Urbana–Champaign, Urbana, Illinois 61801

Conceptual in-space transfer stages, including those using solar electric propulsion and chemical propulsion with aerobraking or aerocapture assist at Mars, were evaluated. Roundtrip Mars sample return mission vehicles were analyzed to determine how technology selections influence payload delivery capability. Results show how specific engine, thruster, propellant, capture mode, trip time, and launch-vehicle technology choices would contribute to increasing payload delivered to Mars or decreasing the size of the required launch vehicles. Low-thrust trajectory analyses for solar-electric transfer were generated with the SEPTOP code.

I. Introduction

MARS sample return (MSR) mission in-space transfer craft capable of delivering payloads to, and returning payloads from, Mars over the years 2009–2018 were investigated. Results show how propulsion system, propellant, trajectory, trip time, and launch-vehicle choices affect delivered payload capabilities. Chemical propulsion MSR spacecraft, using five different propellant combinations were evaluated. These are 1) nitrogen tetraoxide (NTO)/hydrazine (N_2H_4), 2) oxygen (O_2)/hydrazine, 3) oxygen/methane (CH_4), 4) fluorine (F_2)/hydrazine, and 5) oxygen/hydrogen (H_2). These chemical propulsion transfer stages are compared to solar-electric-propulsion (SEP) MSR transfer stages using ion or Hall-thruster technology. One of the objectives of the study was to determine how much payload each of these various systems could boost to Mars for a range of launch-vehicle capabilities. MSR trajectory events are shown in Fig. 1. The chemical propulsion stages presented herein capture at Mars either propulsively or aerodynamically; the Mars lander payload separates previous to Mars capture or, alternatively, separates after capture with the transfer stage into a 400-km circular low mars orbit (LMO). Once the lander surface sampling mission is completed, the Mars ascent stage ascends to LMO with the small sample payload canister. The MSR transfer stage, waiting in LMO, rendezvous with the ascent stage and retrieves the sample module. Once secured, the transfer stage waits in LMO until the next minimum-energy Earth return opportunity. At Earth arrival, the sample payload canister, in its reentry capsule, separates from the transfer stage and returns to Earth via direct entry while the transfer stage is expended. In this study, Mars lander payload is either set to a reference value or is a variable to be optimized consistent with constraints, such as launch-vehicle capability. In all cases, a 150-kg sample module/reentry capsule is collected in LMO and returned to Earth. The total duration of the MSR mission is about three years; typically 500- to 600-day stays are required at Mars before the next minimum energy Earth return departure window opens.

Presented as Paper 2004-3807 at the AIAA/ASME/SAE/ASEE 40th Joint Propulsion Conference, Ft. Lauderdale, FL, 11–14 July 2004; received 13 October 2004; revision received 23 March 2005; accepted for publication 7 April 2005.

*Third Generation Space Technology Lead, MC JV-03, Transformational Space Systems, 950 Explorer Boulevard. Associate Fellow AIAA.
†System Engineer, Engineering and Technology Section, 675 Discovery Drive, Suite 300. Associate Fellow AIAA.
‡Associate Professor, MC 236, Department of Aerospace Engineering, 306 Talbot Laboratory. Associate Fellow AIAA.
§Graduate Student, MC 236, Department of Aerospace Engineering, 327 Talbot Laboratory.

II. Solar-Electric-Propulsion Vehicle Modeling

For generating optimal low-thrust trajectories for the SEP concepts, the SEPTOP[1,2] low-thrust trajectiory optimization tool was used. The trajectory optimization process includes launch-vehicle injected mass capability as a function of trajectory energy [hyperbolic velocity (V_{hp}^2)] $C3$ as an optimization constraint. SEPTOP was utilized to generate the interplanetary trajectories for a variety of relevant launch dates, trip times, departure $C3$s, power levels, and thruster combinations. SEP transfer stage propellant load, delta-velocity (delta-v), thruster operation time, and thruster throttling and sequencing data are generated as well. Specific thruster models are imbedded into the propulsion system modeling, thereby allowing the investigation of detailed issues such as the effect of available array power on the thrust magnitude and thruster efficiency.

SEPTOP MSR cases were run for a variety of $C3$s; for these low-thrust trajectories, payload for a given Earth departure opportunity is in part a function of power level, specific impulse I_{sp}, and launcher capability. In SEPTOP, constraints can be placed on major system elements such as the maximum power output from the solar arrays through feathering and the maximum and minimum thruster operational power levels. For all cases a redundant thruster, power processing unit (PPU), propellant management string, and digital control interface unit (DCIU) are carried. SEP MSR stage contingencies included a 10% propellant margin and a 30% dry mass growth allowance (except 5% on thruster mass).

SEP stage redundancies included a 15% reduction in PPU radiator radiant intensity caused by view onto solar array, and a propulsion system duty cycle: 95% of baseline. SEP attitude control system (ACS) is provided by the ion propulsion system (IPS) during its low-thrust burn periods, and when the IPS is not active (coast periods) ACS is provided by a monopropellant reaction control system (RCS). As mentioned earlier, the SEP MSR IPS uses either ion or Hall-thruster technology; the ion system uses the 6.85-kWe NASA Evolutionary Xenon Thruster (NEXT)[3,4] design with Molybdenum grids. The maximum I_{sp} of this thruster is 4116 s. This compares to

Table 1 Baseline SEP stage power and propulsion system summary

System	Allocation
Power	20–45 kWe, but for results presented herein 22 kWe at 1 AU[a] end of life; 250-We spacecraft bus housekeeping power
Array	Multijunction GaAs arrays; ultraflex design; 23% cell efficiency
Thrusters: ion	2–4 thrusters with 1 spare; 6.85 kWe @ 4116 s I_{sp}; NEXT design; molybdenum grids
Thrusters: Hall	2–4 thrusters with 1 spare; 9.95 kWe @ 3390 s I_{sp}; NASA-173 version 2 design
PPU	2–4 PPUs with 1 spare; cross-strapping PPUs
Radiators	SOA heat-pipe radiators
DCIU	SOA digital control interface unit with 1 spare
Tank and propellant	Tank fraction = 5%; supercritical Xe propellant, 5% ullage
Propellant management	NEXT design
Margins	10% propellant; 30% dry mass, 5% array power, 12% array area

[a]AU = astronomical unit.

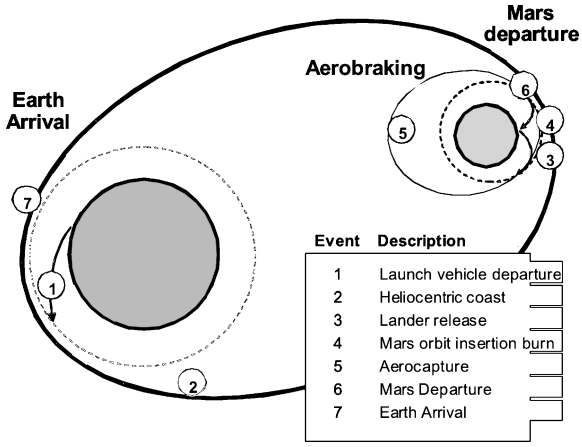

Fig. 1 Mission trajectory events.

the NSTAR ion program thrusters, which demonstrated maximum thruster power of 2.5 kWe. The Hall system uses the 9.95-kWe, 3390-s I_{sp} NASA-173 version 2 design.[5–7] A Hall thruster of this type has achived a 1000-h life test at high power. Currently, Hall thrusters of up to 100 kWe are under development.

PPUs,[8] presently in development under the NEXT program, convert power from the solar array and deliver electrical power at proper voltage and current to the thruster array. This design uses state-of-the-art heat-pipe radiators. SEP xenon tank mass fraction is 5%, and tank ullage volume fraction is 5%. The tanks hold supercritical xenon propellant at a density of 2344 kg/m^3 and a pressure of 34.5 MPa (5000 psia). Large, high-efficiency solar photovoltaic arrays provide power for propulsion and vehicle housekeeping (with the exception of battery power that must be provided for array deployment). The UltraFlex arrays use triple-junction gallium arsenide (GaAs) cells with an efficiency of 23% at the beginning of the mission. An array area increase of 2% is added per year for end-of-life requirements and an additional 10% is added for margin. Two-hundred-fifty We is used for spacecraft housekeeping power throughout the duration of the mission. Spacecraft bus, structures, and mechanisms mass are based on historical data for actual spacecraft. A representative SEP MSR transfer stage of this type weighs about 860 kg dry and 1560 kg wet not including its outbound and inbound payloads. Table 1 contains a summary of the major SEP specifications.

III. Chemical Propulsion Vehicle Modeling

For the high-thrust chemical propulsion transfer stages, published trajectory data are used.[9] Fixed values for Earth departure $C3$, Mars arrival hyperbolic velocity V_{hp}, and Mars departure $C3$ are used, as are midcourse correction and Earth divert maneuver values. Mars capture and departure chemical propulsion system models consist of experience-based data in the form of curve fits of historical data and physics-based models. For example, the composite overwrap tank model is scaled from the Advanced X-ray Astrophysics Facility (AXAF) vehicle's composite tank. The baseline chemical capture stage consists of three main pressure-fed engines of nominally 0.69-MPa (100-psia) chamber pressure with nozzle expansion ratio of 200:1. Main engines are sized for a thrust corresponding to an initial vehicle acceleration of 0.5 at the onset of Mars orbit capture thrusting. Other elements include the thrust-vector-control system, thermal conditioning, pressurization system, and the RCS. I_{sp} values used for the five propellant combinations (NTO/N_2H_4, O_2/N_2H_4, O_2/CH_4, F_2/N_2H_4, and O_2/H_2) are 330, 343, 344, 380, and 420 s, respectively.

Lightweight tanks are operated with tank pressures of 1.72 MPa (250 psia). Thermal conditioning is supplied to tanks, lines, valves, and thrusters. The pressurization system consists of high-pressure, regulated gaseous He with redundant propellant management system controllers. General MSR chemical stage contingencies included a 3.0% propellant margin, a 30% dry mass margin, and a 2.0% gravity loss penalty for all propulsive burns. Electric power is provided by batteries and a 1-kW array. The structural mass calculations are based on historical data for actual planetary spacecraft. The RCS for the chemical stages consisted of 16 hydrazine monopropellant thrusters operating at 220 s I_{sp}. The RCS delta-v budget consisted of 20 m/s at Mars capture for maintaining final parking orbit, 10 m/s each for three other events (Earth and Mars departure, Earth arrival), 30 m/s for course correction and aimpoint maneuvers (each leg), and 40 m/s for the transfer stage Earth divert maneuver.

Aerocapture assumptions of the chemical vehicles consisted of setting the initial brake mass to 20% of total captured mass (including aeroshell). (Values of 10, 15, 25, and 30% are also evaluated.) A 50-m/s propulsive delta v is applied postaerocapture for the Mars periapsis raise maneuver and other corrections, as well as a 85-m/s delta v for the final circularization. Table 2 contains a summary of the major chemical stage specifications.

IV. SEP Configuration and Launch Vehicles

A conceptual Earth–Mars–Earth SEP transfer stage is illustrated in Fig. 2. The vehicle pictured features dual UtraFlex solar arrays, a spacecraft bus with the necessary avionic, thermal, propellant management, and other subsystems, and the IPS (Xenon ion thrusters, PPUs, and DCIU). A Mars lander payload (housed in

Table 2 Chemical stage systems summary

System	Allocation
Propulsion main	Three pressure-fed engines, 0.69 MPa (100 psia) chamber pressure; 200:1 ratio nozzle; vehicle T/W = 0.5 at onset of Mars capture burn[a]
Propellants evaluated	NTO/ N_2H_4, O_2/ N_2H_4, O_2/ CH_4, F_2/ N_2H_4, and O_2/H_2, 330, 343, 344, 380, 420 s I_{sp}
Propulsion RCS	16 hydrazine monopropellant thrusters; 220 s I_{sp}
Aerobrake	Nominally 20% of total Mars captured mass (including aeroshell)
Tank and propellant	Composite overwrap tank scaled from AXAF; 1.72 MPa (250 psia)
Power	1-kWe array, battery
Margins	3% propellant; 30% dry mass; 2% gravity loss on all delta v

[a]T/N = thrust-to-weight ratio.

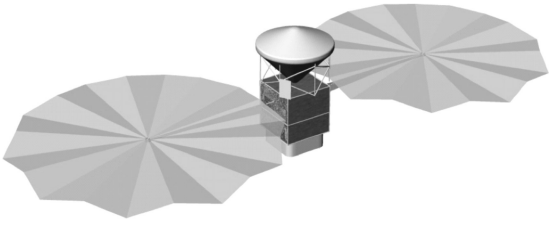

Fig. 2 SEP MSR transfer stage with direct-entry lander module.

its Mars direct aeroentry shell) is shown with its adapter structure at the top of the illustration. In Fig. 3 the SEP vehicle is shown stowed in its launch vehicle shroud.

Medium-class launch vehicles and their injection capabilities to $C3$s of 0 and 10 km^2/s^2 are listed in Table 3. The payload values at $C3 = 10$ became the allowable initial masses for the chemical transfer stages. All launcher values contained a 2% margin. As mentioned earlier, a range of $C3$s was evaluated for the SEP vehicles.

V. Mission and Trajectory Design

A. Mars Mission Trajectory Options

Mars trajectory options open to the mission designer are listed in Fig. 4. In this analysis, only results for which the launcher provided Earth departure $C3$s of greater than zero are presented. Two Mars capture modes are evaluated. In the first, lander direct entry (LDE), the Mars lander separates previous to capture and continues on to a direct entry landing. In the second, the lander is captured with the orbiter into LMO (labeled LCO). Other selections include conjunction class trajectories and return via direct Earth intercept. A circular 400-km LMO was chosen as was sample return via Mars orbit rendezvous.

Table 3 Launch-vehicle payload capabilities

Launch vehicle	Injected mass $C3 = 0$ LV margin 0%, kg	Injected mass $C3 = 10$ LV margin 2%, kg
Atlas-V 431	5536	4527
Atlas-V 421	4880	3993
Delta-IV 4450	4583	3612
Delta-IV 4240	4075	3212

Fig. 3 SEP vehicle in stowed position.

B. Earth Departure Requirements

Figure 5 provides a summary of the departure energies ($C3$) required for each optimal Mars mission[4]; these are not constrained on trip time or Mars arrival velocity. There is a rapid increase in departure energy required for the 2020 Earth departure opportunity. The minimum energy transfer in this 2020 case is a type I; hence the higher energy and shorter mission duration. The 2018 opportunity is also type I; all others are type II. (Type I refers to trajectories in which the heliocentric transfer angle is less than 180 deg; type II angles are greater than 180 deg.) Variations in $C3$s can be caused by many causes: the relative positions of the planets, the plane change required into the transfer orbit, the velocities of the planets, and the eccentricities of the orbits.[10] Time of flight in days is listed for each opportunity, as are Mars arrival V_{hp} and trajectory type.

In data presented here, all of the chemical transfer stages featured a fixed launch injection to $C3 = 10$ km^2/s^2. This departure energy is chosen because it covers all but the three most difficult Earth–Mars opportunities (2020, 2022, and 2024) in the period under investigation. For the chemical stages, fixed Mars arrival V_{hp} values of 3.0 km/s are used for the same reason, as are Mars departure V_{hp} values of 3.1 km/s; these values are slightly higher than the optimized trajectory values for the 2011–2018 missions[9] and are chosen to cover these opportunities with some velocity margin. Over that period, outbound trip times vary from 236 to 328 days; arrival V_{hp} range from 2.78 to 2.99 km/s. The 2009 departure optimizes at about $C3 = 10$ km^2/s^2; once injected, the chemical stage would coast for 327 days until its Mars encounter. Because of their ballistic trajectories, the chemical stages only require Mars capture and departure burns (aside from small midcourse and correction burns). The higher I_{sp}, low-thrust SEP vehicles were configured to thrust continuously during a portion of the outbound transit and for this reason were in the simulations often injected to $C3$ less than that which would be optimal for a ballistic transfer departing the same year. Thus SEP outbound trip times are typically longer, varying from about 1.0 to 2.0 years (including Mars spiral down time which takes several months) as compared to the 0.7 to 0.9 year trip times typical of the ballistic trajectories. It is advantageous, for maximizing the payload delivered to Mars, for the electric vehicle's high I_{sp} to displace the lower I_{sp} of the launcher's upper stage; the disadvantage is increased trip time.

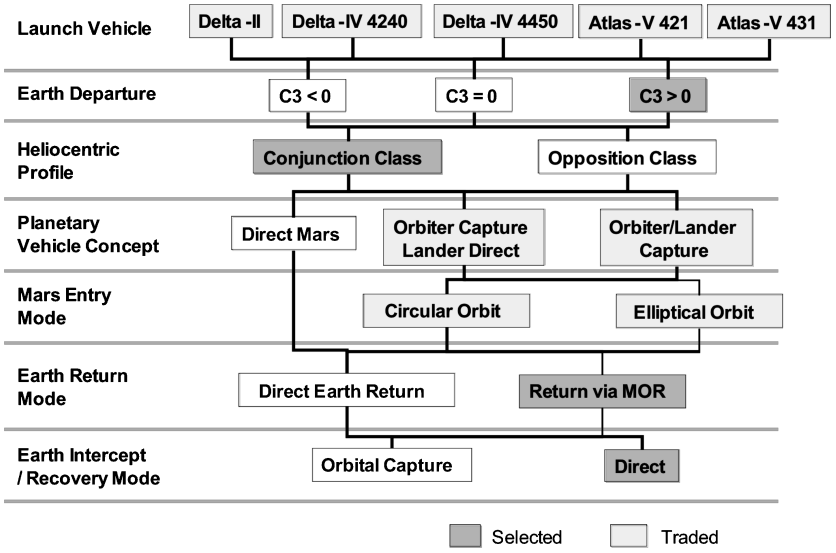

Fig. 4 Mars trajectory options.

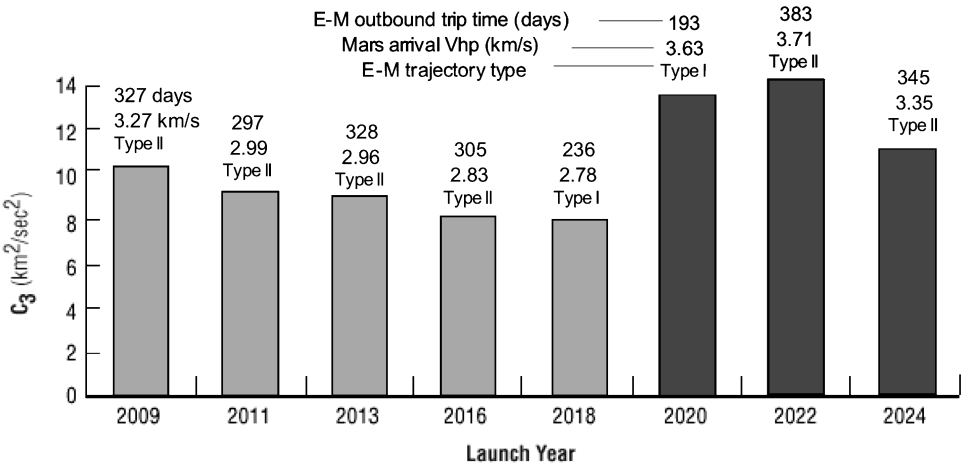

Fig. 5 Earth–Mars outbound transfer departure energies and trip times.

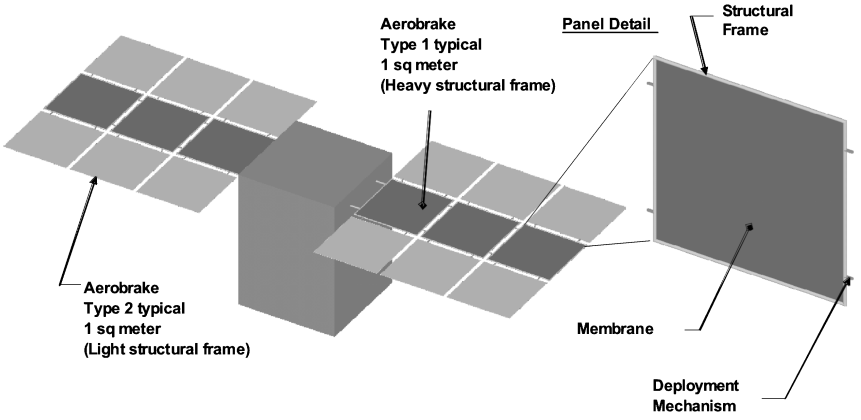

Fig. 6 Aerodynamic panels for aerobraking.

Table 4 Chemical transfer stage delta-v budgets (m/s)

Maneuver	All propulsive	Propulsive/ aerobraking	Aerocapture
Outbound leg			
Outbound midcourse correction, m/s	30	30	30
Mars arrival ($V_{hp} = 3.0$)			
MOI propulsive capture	2261	1097	0
Corrective maneuvers	0	101	135
Rendezvous (with ascent age)	100	100	100
Mars departure ($V_{hp} = 3.1$)			
Trans Earth injection	2315	2315	2315
Inbound leg			
Inbound midcourse correction	30	30	30
Earth divert	40	40	40
G losses: 2% of total	96	74	53
Total	4872	3787	2703
Percentage	100	78	55

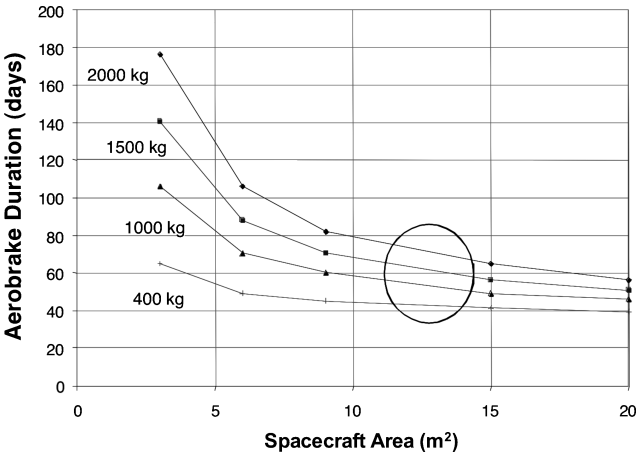

Fig. 7 Aerobrake maneuver duration vs panel area.

C. Chemical MSR Roundtrip Delta-Velocities

MSR roundtrip transfer delta-v requirements are listed in Table 4 for three categories corresponding to Mars capture mode. In each case Mars entry V_{hp} is 3.0 km/s. The first option is all-propulsive capture into LMO. Capture delta-v required is 2261 m/s into the LMO of 400 km circular. The second option, referred to as chemical-aerobrake (Chem-Ab), is defined by an initial propulsive capture into a 400 × 33,000 km, 24-h period highly elliptical Mars orbit (HMO). 1097 m/s delta-v is required to propulsively capture into HMO. From that orbit the spacecraft aerodynamically decelerates during each successive pass through the Mars atmosphere (at periapsis), losing orbital energy until it is circularized to 400 km. About 10 m/s of propulsive delta-v is applied for corrections during and after the maneuver.

Aerodynamic panels, deployed to increase aerodynamic drag during the maneuver, are shown in Fig. 6. Various aerobrake areas can be achieved through combinations of type 1 and type 2 panels, which vary in the weight of their structural frames. Stowed aerobrake panels package into a 1 × 1 × 0.13 m volume. In Fig. 7, aerobrake duration is plotted vs panel area. A panel area of 12 m^2 was chosen for reasonable aerobrake duration; at that level the maneuver can be accomplished in 60–90 days.

In the chemical-aerocapture (Chem-Ac) option, the third evaluated, the MSR craft targets a Mars atmospheric entry point at

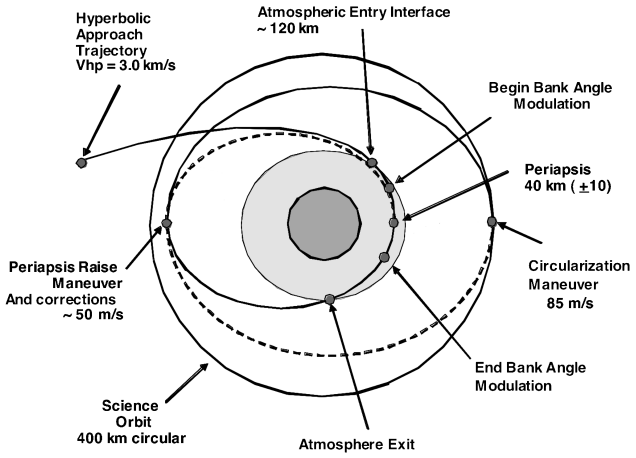

Fig. 8 Mars aerocapture parameters.

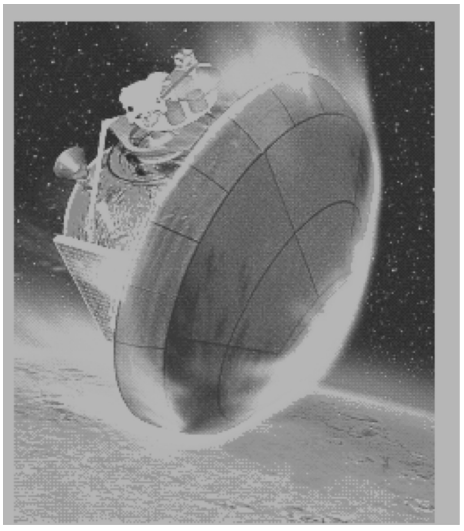

Fig. 9 Mars aerocapture.

120-km altitude and conducts a full, single-pass aerocapture maneuver, followed by a propulsive burns of 135 m/s to raise periapsis to circular LMO and to conduct corrective maneuvers. Aerocapture saves 1097 m/s of delta-v compared to the aerobraking case and 2261 m/s compared to the all-propulsive case (Table 4). The total MSR roundtrip delta-v budgets for the aerobraking and aerocapture cases, as a percentage of the all-propulsive case, are 78 and 55%, respectively. The budgets include a 100-m/s delta-v rendezvous maeuver for the transfer stage to close with the ascent stage sample payload module in LMO.

D. Mars Aerocapture Parameters

A representative Mars aerocapture path is shown in Fig. 8; the vehicle's atmospheric entry interface is set to 120-km altitude; at this point the vehicle begins bank-angle modulation for steering to remain within the prescribed flight corridor. Mars closest approach occurs at an altitude of 40 km, the periapsis of the aeropass ellipse; once out of the atmosphere and at apoapsis, a periapsis raise maneuver and correction burn of 50 m/s is applied. Later, an 85-m/s circularization burn completes the transition to the final 400-km circular LMO. Aerocapture provides the full velocity reduction required for capture before exiting the atmosphere in a single pass. Mars aerocapture is represented in Fig. 9.

VI. MSR SEP Transfer Stage Design

A. SEP Solar-Array Information

Large, high-efficiency solar photovoltaic arrays provide propulsion power and vehicle housekeeping power (with the exception

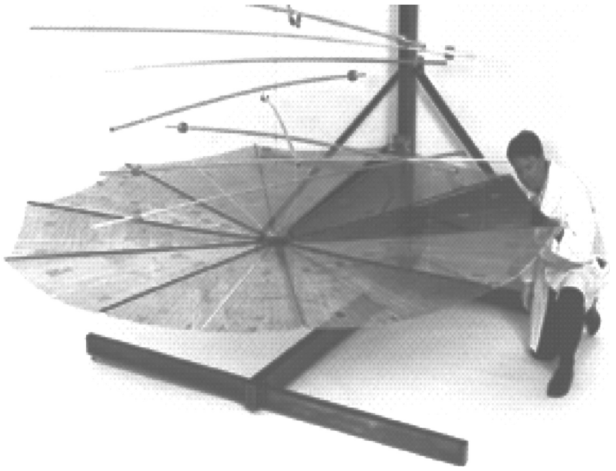

Fig. 10 UltraFlex solar-array panel.

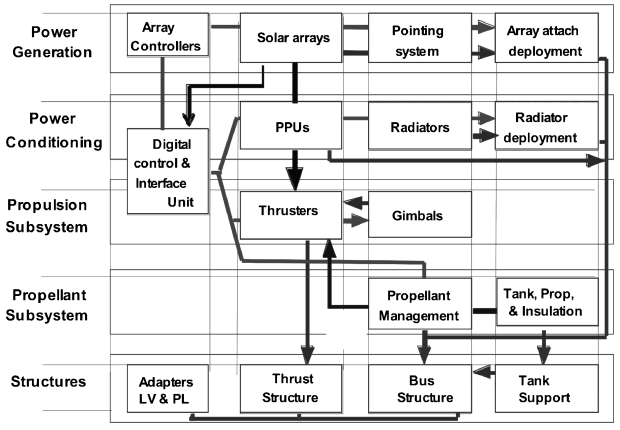

Fig. 11 SEP elements modeling diagram.

of battery power that must be provided for array deployment). An articulation of the arrays, in one axis relative to the sun, provides array feathering to control array temperature and prevents the solar flux from exceeding a maximum allowable value on the arrays. The UltraFlex arrays represent the present state of the art in lightweight solar-array technology. A typical array element is shown in Fig. 10.

Solar flux at Earth (1.0) AU is 1358 W/m^2; at Mars, a distance of about 1.5 AU, flux decreases to 40% of its 1.0 AU value (604 W/m^2). In the analyses array power levels are varied from 20 to 45 kWe, though data are shown only for a 22-kWe nominal power level system. Array mass, however, is based on the combined additions of a 5% power margin (24.2 kWe) and a 10% area margin to provide further conservatism. Major SEP elements modeled are shown in Fig. 11.

B. SEP Ion Thrusters

The SEP stage includes an array of two to four NEXT ion thrusters rated at 6.85 kWe each. The thruster elements consist of a set of thrusters, gimbals, actuators, a DICU, sun shield and support structure. A NEXT thruster is pictured in Fig. 12. In Fig. 13 the NASA-173 version 2 Hall thruster is shown. The SEPTOP simulation throttles the thrusters as required to attain minimum propellant loading necessary for given mission, power level, and thruster characteristics. NEXT and NASA-173 throttling performance is calculated using supplied I_{sp} vs power throttle tables; Fig. 14 shows an example taken from Ref. 11.

Ion thrusters suffer from low thrust density (available thruster per unit exhaust area) because the maximum ion current density that can be sustained is limited by space-charge distortions of the applied electric field. One advantage of the Hall thruster compared to an electrostatic ion engine is that as the plasma in the Hall

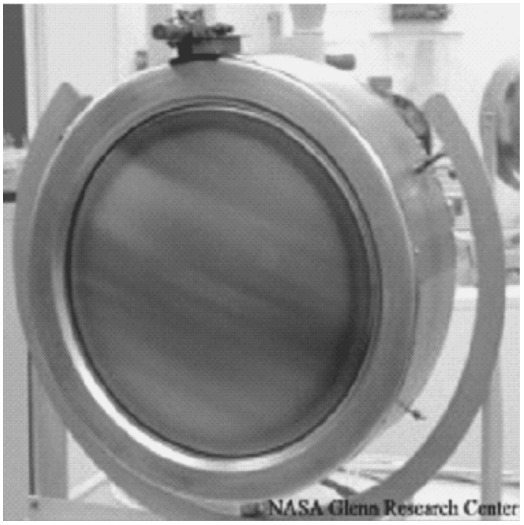

Fig. 12 NASA Evolutionary Xenon Ion Thruster (NEXT).

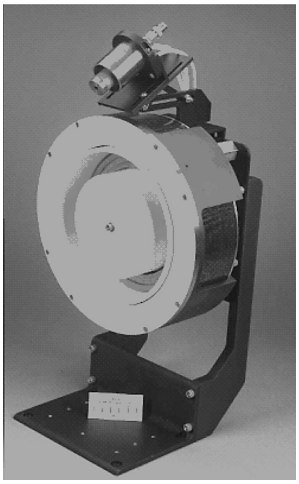

Fig. 13 NASA-173 version 2 Hall thruster.

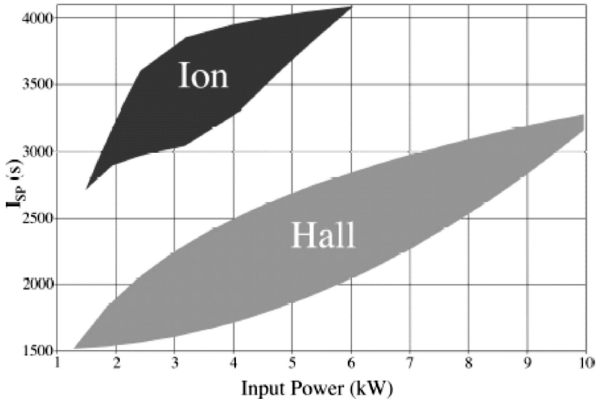

Fig. 14 Example ion and Hall thruster I_{sp} vs input power throttling table.

effect thruster remains substantially neutral because of the presence of the electrons that constitute the Hall current they are able to sustain higher ion current densities and hence offer greater thrust densities.

VII. Comparative Analysis

A. MSR Chemical Propulsion Stages

Launch-vehicle injected mass is plotted vs propellant type and Mars orbit capture mode in Figs. 15 and 16. The NTO/N_2H_4 Chem-Ab transfer stage serves as the reference vehicle for comparison purposes. Allocations for stage inert, propellant, aerocapture brake, inbound payload, and outbound (lander) payload masses are shown.

For all of the data presented in Fig. 15, Mars lander payload is fixed at a 1200-kg reference value, lander release occurs previous to Mars capture (LDE mode), and chemical stage mass is that which is to be determined. The data grouped on the left-hand side of the plot are aerobraking (Chem-Ab) cases; for these it can be seen that 1) all propulsion types except O_2/CH_4 and O_2/H_2 injection masses are within Atlas-V 431 capabilities; 2) only F_2/N_2H_4 injected masses fall within Atlas-V 421 capabilities; and 3) O_2/H_2 inert mass is comparatively high because of the cryocooler mass requirements for storing H_2 for the Mars capture and departure burns. O_2/H_2 propulsion does not allow any payload to be delivered.

The data on the right-hand side of Fig. 15 are aerocapture (Chem-Ac) cases:

1) All propulsion types except O_2/H_2 injection masses fall within Atlas-V 431 capabilities.

2) NTO/N_2H_4 and O_2/N_2H_4 vehicle injected masses fall within Atlas-V 421 capabilities.

3) Only F_2/N_2H_4 injected mass falls within Delta-IV 4450 capabilities.

4) Aerocapture allows ~500-kg reductions in injected mass compared to aerobraking.

Fluorine has reactivity and toxicity issues, though fluorine engines were tested successfully by NASA and the U.S. Air Force during engine development programs in the 1960s and 1970s. The applicability of this propellant for spaceflight is presented in Refs. 12–14.

For all data shown in Fig. 16, Mars lander mass is variable, and injected mass is fixed at the Atlas-V 421 value. Lander release occurs previous to the transfer stage capture:

1) For chemical-aerobrake, lander masses of approximately 1000, 900, 1300, and 400 kg are achieved for NTO/N_2H_4, O_2/N_2H_4, F_2/N_2H_4, and O_2/CH_4, respectively.

2) O_2/H_2 propulsion does not allow any payload to be delivered.

3) For aerocapture, lander masses increase to approximately 1500, 1400, 1600, and 1100 kg for the NTO/N_2H_4, O_2/N_2H_4, F_2/N_2H_4, and O_2/CH_4 vehicles, respectively.

4) Aerocapture allows for lander mass increases of 300 to 700 kg compared to aerobraking.

In Fig. 17, both Mars lander mass and injected mass are variable. In each case exclusive use is made of aerocapture at Mars, LDE, and NTO/N_2H_4 propulsion. Lander masses of approximately 900, 1200, 1500, and 1900 kg are achieved for Delta-IV 4240, 4450, Atlas-V 421, and 431 capabilities.

In Fig. 18, chemical stage injected mass is plotted vs aerocapture brake mass percentage. The mass captured includes the mass of the

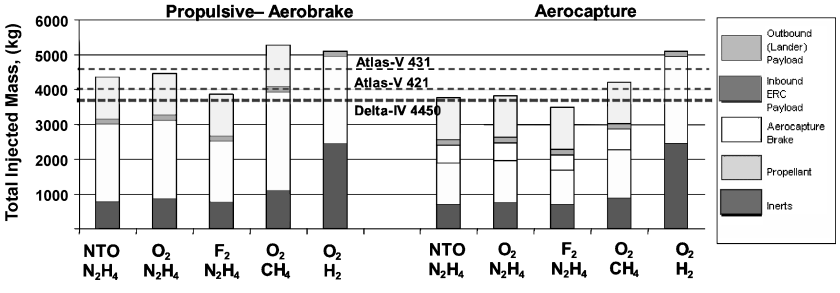

Fig. 15 MSR injected mass for 1200-kg Mars lander/chemical transfer stage combination.

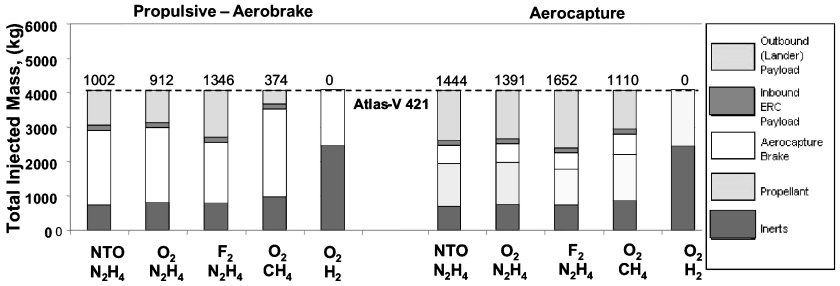

Fig. 16 MSR chemical stage Mars payload and injected mass for Atlas-V 421.

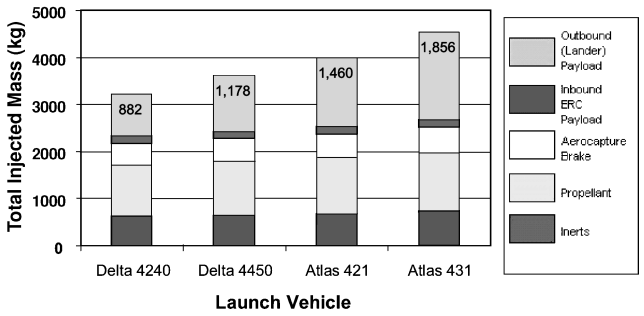

Fig. 17 NTO/N_2H_4 Chem-Ac stage injected mass vs launch vehicle.

aeroshell. Lander mass is fixed at 1200 kg, LDE mode is used, and propulsion is NTO/N_2H_4:

1) Aerocapture shell mass percentages of 30% (or greater) show no advantage over aerobraking.

2) At a brake percentage of 25%, injected mass is within the capability of the Atlas-V 421.

3) At brake percentages of 15% and lower, injected masses are within the capability of the Delta-IV 4450.

B. MSR SEP Propulsion Stages

SEPTOP trajectories were generated for a wide variety of injected $C3$ values; the SEP data shown in Fig. 19 are injected by a Delta-IV 4240 to $C3 = 5.5$ km^2/s^2. Data for this 22-kWe vehicle with two NEXT thrusters are for a 2009 departure; 2009 is a year in which the optimum $C3$ for the ballistic chemical stages is 10 (Fig. 5). Optimal $C3$s for the other years in the 2011–2018 period are less than 10; payloads would be higher for these less difficult opportunities. Columns 2 and 3 of Fig. 19 show Chem-Ac and Chem-Ab systems injected with the larger Delta-IV 4450. The Delta-IV 4240 can boost to a $C3$ of 5.5 about the same mass (3660 kg) that the Delta-IV 4450 can boost to a $C3$ of 10. Thus each of the three transfer stage/payload combinations in Fig. 20 (SEP, Chem-Ac and Chem-Ab) weigh on the order of 3600 kg, but the SEP is launched on the smaller, less costly launcher to the lower $C3$. Although this one comparison is valid for 2009, it is generally indicative of the relative differences in performance afforded by these technologies in other years. Observations drawn from Fig. 19 include the following:

1) The 2009 22-kWe SEP ion system can deliver a lander of about 1900 kg when injected via the Delta-IV 4240 to a $C3 = 5.5$ km^2/s^2.

2) Chem-Ac and Chem-Ab can deliver landers of about 1200 and 800 kg, respectively, when injected via the larger Delta-IV 4450 to the higher $C3 = 10$ value.

3) The SEP payload advantage is about 700 and 1100 kg vs Chem-Ac and Chem-Ab, respectively.

4) The high I_{sp} (4612 s) of the SEP allows it to conduct the mission with significantly less propellant as compared to the chemical vehicles, the I_{sp} of which is an order of magnitude lower (330 s).

5) 2009 22-kWe SEP ion outbound heliocentric trip time to Mars sphere of influence is 1.3 years, about one half-year longer (on both the outbound and inbound legs) than the chemical vehicles (which require about 0.9 years).

Table 5 SEP power budget (22-kWe array)

Power budget	Earth	Mars
Array, AU	1.00	1.50
Sunlight intensity, W/m^2	1358	604
Array area w margin, m^2	96.8	96.8
Array area required, m^2	70.4	70.4
Array power for costing, kWe	24.2	——
Array power, kWe	22.0	9.78
Into IPS		
Housekeeping power, kWe	0.25	0.25
Power feathered, kWe	7.32	0.0
Act max power IPS, kWe	14.43	9.53
Act max into PPUs, kWe	14.36	9.48
Act max Po thrusters, kWe	13.70	8.97
Thrust total, N	0.47	0.31

Table 6 SEP mass (22-kWe array)

No.	Element	Unit, kg	Margin, %	Total, kg
1	Power gen	104	30	135
2	Power distribution	22	30	29
3	Propulsion	151	5	159
4	Tankage and feed sys	60	30	78
5	Thermal control	18	30	24
6	Structure	113	30	147
7	Mechanism	15	30	20
8	Adapters	42	30	55
9	Acs	42	30	54
10	Other	9	30	12
11	Telecom, command and data handling	32	30	42
12	Guidance, navigation, and control	20	30	26
13	Other	18	30	23
14	Rendezvous instr suite	40	30	52
——	Dry mass	——	——	856
15	Reserve	——	——	64
16	Propellent inbound	——	——	152
17	Rendezvous	——	——	3
18	Outbound	——	——	485
——	wet mass	——	——	1560
19	Payload outbound	——	——	1906
20	Inbound	——	——	194
21	Launch mass	——	——	3660

6) A 0.4-year spiral-down time is also required of the SEP, though this occurs after lander release and so would not delay the surface mission. A similar spiral-up period is required.

Power and mass values for the 22-kWe SEP vehicle are given in Tables 5 and 6. Other SEP ion- and Hall-thruster cases were run at differing power levels (up to 45 kWe); some of these cases also resulted in reduced launch requirements when compared to the Chem-Ac and Chem-Ab systems. The use of power levels higher than 22 kWe typically reduced trip time, but, depending on several factors, less payload mass might be delivered to Mars because of the increase in stage inert mass. A payload-mass-optimal power level for SEP MSR missions was not determined. Results also show that at equivalent power levels, the Hall system, with less I_{sp} than the ion

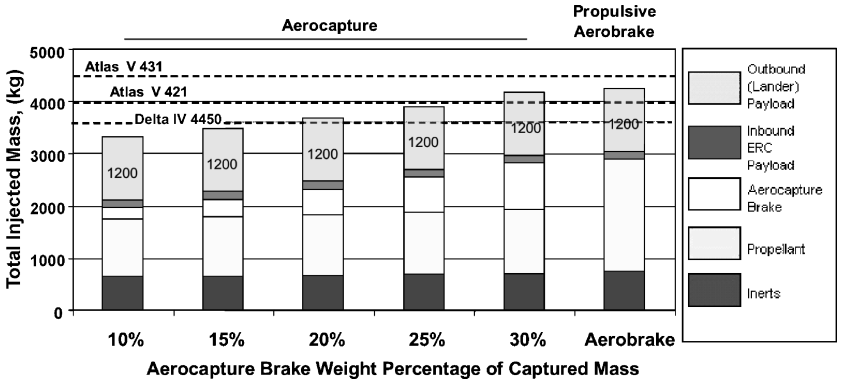

Fig. 18 MSR injected mass vs aerocapture brake mass percentage.

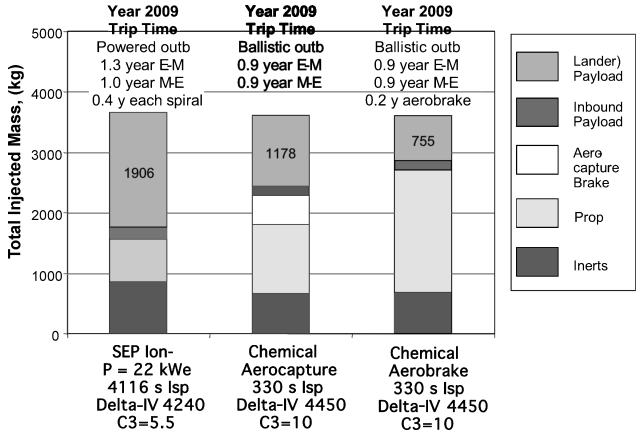

Fig. 19 SEP, Chem-Ac, and Chem-Ab comparison data.

system, will require more stage mass to deliver the same payload but would do so in less time.

VIII. Conclusions

Roundtrip Mars sample return vehicles were analyzed to determine how specific technology selections influence payload delivery capability. Although there is not space in this paper to show all of the performance data that were generated, the following general statements summarize the findings. These conclusions only apply to the MSR missions and ground rules of the type described in this paper. Comparison statements are referenced to the baseline NTO/N_2H_4 Chem-Ab vehicle. Results indicate the following:

1) Cryogenic O_2/H_2 and O_2/CH_4 propulsion technologies result in decreased Mars payload masses. Cryocooler mass negates the I_{sp} advantage of these two propellants for this mission class.

2) Advanced fluorine engine technology provides modest increases to deliverable Mars payload masses.

3) Aerocapture technology increases Mars payload masses significantly (if brake mass is 20% or less of the total captured mass). Aerocapture technology at brake mass fractions of 30% or above does not provide payload increases as compared to aerobraking.

4) SEP ion technology shows the potential for increased Mars payload masses most significantly, at the cost of increased trip times. Trip time is in part a function of power level and mission year. Increasing power level to reduce trip time can diminish somewhat SEPS payload delivery capability. The optimal SEP power level for MSR is dependent on several factors, and a "best value" was not determined.

Acknowledgments

Results presented here were generated under the NASA In-Space Technology Assessment contract. Special thanks go to Les Johnson, Manager of NASA MSFC In-Space Propulsion, and Randy Baggett, Program Manager of NASA MSFC Next Generation Electric Propulsion program, for providing direction for this work. Our many thanks to Michael Cupples, Tom Percy, Gordon Woodcock, Dave Byers, Gwen Artis, and Melody Hermann.

References

[1]Sauer, C., Jr., "Optimization of Multiple Target Electric Propulsion Trajectories," AIAA Paper 73-205, Jan. 1973.

[2]Sauer, C., Jr., "Solar Electric Propulsion Performance for Medlite and Delta Class Planetary Missions," American Astronautical Society, AAS Paper 97-726, Aug. 1999.

[3]NASA Research Announcement Proposal Information Package Next Generation Ion Engine Technology, NASA, June 2003, Sec. A.9.2.

[4]Patterson, M., Thomas, M., Foster, W., Rawlin, J., Roman, V., Robert, F., and Soulas, G. "Development Status of a 5/10-kW Class Ion Engine," AIAA Paper 2001-3489, July 2001.

[5]Manzella, D., Jankovsky, R., and Hofer, R., "Laboratory Model 50 kW Hall Thruster," AIAA Paper 2002-3676, July 2002.

[6]Jacobson, D., and Manzella, D., "50 kW Class Krypton Hall Thruster Performance," AIAA Paper 2003-4550, 2003.

[7]Fiehler, D., and Jankovsky, R., "The Influence of Current Density and Magnetic Field Topography in Optimizing the Performance, Divergence and Plasma Oscillations of High Specific Impulse Hall Thrusters," 28th International Electric Propulsion Conf., IEPC-03-142, Toulouse, France, March 2003.

[8]Piñero, L., "Design of a Modular 5-kW Power Processing Unit for the Next-Generation 40-cm ion Engine," 27th International Electric Propulsion Conf., IEPC-01-329, Pasadena, CA, Oct. 2001.

[9]George, L. E., and Kos, L. D., "Interplanetary Mission Design Handbook: Earth-Mars Mission Opportunities and Mars-Earth Return Opportunities 2009-2024," NASA TM-1998-208533, July 1998.

[10]Brown, C. D., *Spacecraft Mission Design*, AIAA, Washington, DC, 1992.

[11]Fiehler, D., and Oleson, S., "A Comparison of Electric Propulsion Systems for Mars Exploration," AIAA Paper 2003-4574, 2003.

[12]Annel, M. A., Kaplan, R. B., and Tuffias, R. H., "Liquid Fluorine/Hydrazine Rhenium Thruster Update," *Proceedings of the 1983 JANNAF Propulsion Meeting*, Publ. 390, Vol. 1, Chemical Propulsion Information Agency, Laurel, MD, 1983, p. 85.

[13]Bond, D. L., "Technology Status of a Fluorine-Hydrazine Propulsion System for Planetary Spacecraft," AIAA Paper 79-0907, March–April 1979.

[14]Donahue, B. D., "Beating the Rocket Equation: Air-Launch with Advanced Chemical Propulsion," *Journal of Spacecraft and Rockets*, Vol. 41, No. 2, 2004, pp. 302–309.

J. Martin
Associate Editor